

IEEE TRANSACTIONS ON GEOSCIENCE AND REMOTE SENSING

A PUBLICATION OF THE IEEE GEOSCIENCE AND REMOTE SENSING SOCIETY



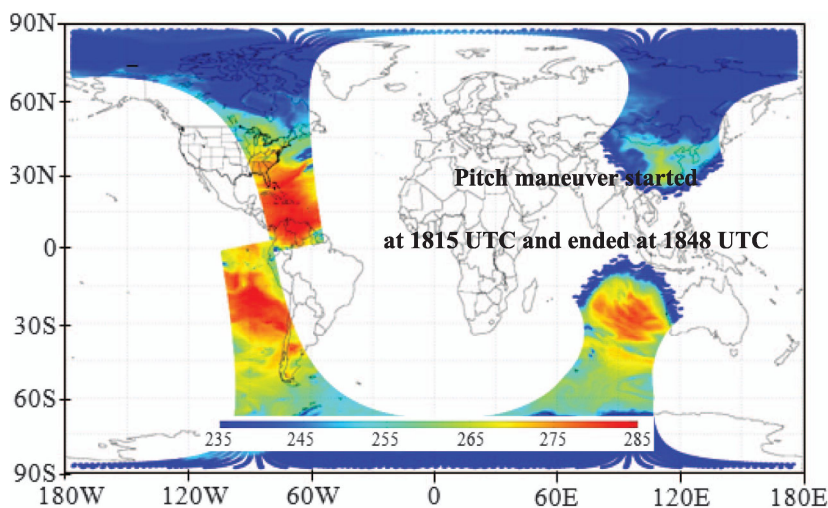
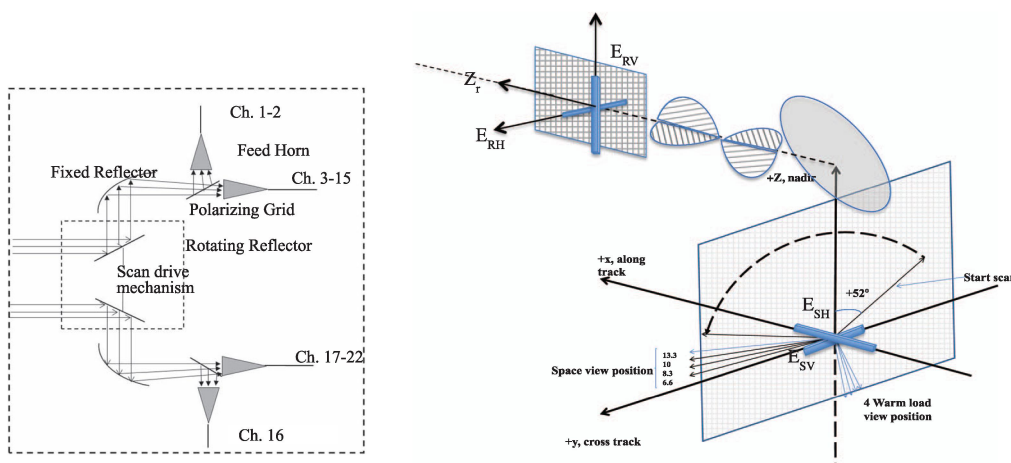
AUGUST 2016

VOLUME 54

NUMBER 8

IGRSD2

(ISSN 0196-2892)



Advanced Technology Microwave Sounder (ATMS) onboard the Suomi NPP satellite. (Left) Schematic of the antenna subsystem. (Right) Sketch plot for polarization direction definition. (Bottom) Orbital brightness temperatures.

IEEE TRANSACTIONS ON GEOSCIENCE AND REMOTE SENSING

A PUBLICATION OF THE IEEE GEOSCIENCE AND REMOTE SENSING SOCIETY



AUGUST 2016

VOLUME 54

NUMBER 8

IGRSD2

(ISSN 0196-2892)

PAPERS

Atmosphere

- Two-Year Comparison of Airborne Measurements of CO₂ and CH₄ With GOSAT at Railroad Valley, Nevada
..... *T. Tanaka, E. Yates, L. T. Iraci, M. S. Johnson, W. Gore, J. M. Tadić, M. Loewenstein, A. Kuze, C. Frankenberg, A. Butz, and Y. Yoshida* 4367
- MST Radars of Chinese Meridian Project: System Description and Atmospheric Wind Measurement *G. Chen, X. Cui, F. Chen, Z. Zhao, Y. Wang, Q. Yao, C. Wang, D. Lu, S. Zhang, X. Zhang, X. Zhou, L. Huang, and W. Gong* 4513

Vegetation and Land

- Radiometric Correction of Airborne Radar Images Over Forested Terrain With Topography
..... *M. Simard, B. V. Riel, M. Denbina, and S. Hensley* 4488
- A Radiative Transfer Model for Heterogeneous Agro-Forestry Scenarios
..... *Y. Zeng, J. Li, Q. Liu, A. R. Huete, G. Yin, B. Xu, W. Fan, J. Zhao, K. Yan, and X. Mu* 4613
- Retrieval of Leaf, Sunlit Soil, and Shaded Soil Component Temperatures Using Airborne Thermal Infrared Multiangle
Observations *Z. Bian, Q. Xiao, B. Cao, Y. Du, H. Li, H. Wang, Q. Liu, and Q. Liu* 4660
- A Local Structure and Direction-Aware Optimization Approach for Three-Dimensional Tree Modeling
..... *Z. Wang, L. Zhang, T. Fang, X. Tong, P. T. Mathiopoulos, L. Zhang, and J. Mei* 4749
- A Novel Hybrid Method for the Correction of the Theoretical Model Inversion in Bio/Geophysical Parameter Estimation
..... *D. Castelletti, L. Pasolli, L. Bruzzone, C. Notarnicola, and B. Demir* 4764

Electromagnetics

- Underground Incrementally Deployed Magneto-Inductive 3-D Positioning Network
..... *T. E. Abrudan, Z. Xiao, A. Markham, and N. Trigoni* 4376
- Scattering From Inhomogeneous Dielectric Cylinders With Finite Length *C. Yang, J. Shi, Q. Liu, and Y. Du* 4555
- Magnetic Induction-Based Positioning in Distorted Environments *O. Kypris, T. E. Abrudan, and A. Markham* 4605
- Assessment of Electromagnetic Absorption of Ice From Ice Core Measurements
..... *A. Zirizzotti, L. Cafarella, S. Urbini, J. A. Baskaradas, and A. Settini* 4758
- Wireless Transmission of MWD and LWD Signal Based on Guidance of Metal Pipes and Relay of Transceivers
..... *W. Li, Z. Nie, and X. Sun* 4855
- Open-Ended Coaxial Probe Technique for Dielectric Spectroscopy of Artificially Grown Sea Ice
..... *S. A. Komarov, A. S. Komarov, D. G. Barber, M. J. L. Lemes, and S. Rysgaard* 4941

(Contents Continued on Page 4366)

| | |
|---|--|
| Hyperspectral Data Processing | |
| Semisupervised Subspace-Based DNA Encoding and Matching Classifier for Hyperspectral Remote Sensing Imagery | <i>A. Ma, Y. Zhong, B. Zhao, H. Jiao, and L. Zhang</i> 4402 |
| Efficient Multiple Feature Fusion With Hashing for Hyperspectral Imagery Classification: A Comparative Study | <i>Z. Zhong, B. Fan, K. Ding, H. Li, S. Xiang, and C. Pan</i> 4461 |
| Spectral–Spatial Feature Extraction for Hyperspectral Image Classification: A Dimension Reduction and Deep Learning Approach | <i>W. Zhao and S. Du</i> 4544 |
| Hyperspectral Image Restoration via Iteratively Regularized Weighted Schatten p -Norm Minimization | <i>Y. Xie, Y. Qu, D. Tao, W. Wu, Q. Yuan, and W. Zhang</i> 4642 |
| Simultaneously Sparse and Low-Rank Abundance Matrix Estimation for Hyperspectral Image Unmixing | <i>P. V. Giampouras, K. E. Themelis, A. A. Rontogiannis, and K. D. Koutroumbas</i> 4775 |
| Dirichlet Process Based Active Learning and Discovery of Unknown Classes for Hyperspectral Image Classification | <i>H. Wu and S. Prasad</i> 4882 |
| A Novel Synergetic Classification Approach for Hyperspectral and Panchromatic Images Based on Self-Learning | <i>X. Lu, J. Zhang, T. Li, and Y. Zhang</i> 4917 |
| Spectral–Spatial Classification of Hyperspectral Images Using ICA and Edge-Preserving Filter via an Ensemble Strategy | <i>J. Xia, L. Bombrun, T. Adali, Y. Berthoumieu, and C. Germain</i> 4971 |
| Hyperspectral Unmixing With Endmember Variability via Alternating Angle Minimization | <i>R. Heylen, A. Zare, P. Gader, and P. Scheunders</i> 4983 |
| Image Processing and Analysis | |
| Detection of Fragmented Rectangular Enclosures in Very High Resolution Remote Sensing Images | <i>I. Zingman, D. Saupe, O. A. B. Penatti, and K. Lambers</i> 4580 |
| A Generalized Metaphor of Chinese Restaurant Franchise to Fusing Both Panchromatic and Multispectral Images for Unsupervised Classification | <i>T. Mao, H. Tang, J. Wu, W. Jiang, S. He, and Y. Shu</i> 4594 |
| Edge-Guided Image Object Detection in Multiscale Segmentation for High-Resolution Remotely Sensed Imagery | <i>Y. Hu, J. Chen, D. Pan, and Z. Hao</i> 4702 |
| Microwave Radiometry | |
| Application of AMSR-E and AMSR2 Low-Frequency Channel Brightness Temperature Data for Hurricane Wind Retrievals | <i>M. Mai, B. Zhang, X. Li, P. A. Hwang, and J. A. Zhang</i> 4501 |
| Disaggregation of Remotely Sensed Soil Moisture in Heterogeneous Landscapes Using Holistic Structure-Based Models | <i>S. Chakrabarti, J. Judge, T. Bongiovanni, A. Rangarajan, and S. Ranka</i> 4629 |
| Spatial Correlations in SMOS Antenna: The Role of Effective Point Spread Functions | <i>J. Martínez, A. Turiel, V. González-Gambau, and E. Olmedo</i> 4906 |
| A Preliminary Evaluation of the SMAP Radiometer Soil Moisture Product Over United States and Europe Using Ground-Based Measurements | <i>J. Zeng, K.-S. Chen, H. Bi, and Q. Chen</i> 4929 |
| Assessment of the SMAP Passive Soil Moisture Product | <i>S. K. Chan, R. Bindlish, P. E. O’Neill, E. Njoku, T. Jackson, A. Colliander, F. Chen, M. Burgin, S. Dunbar, J. Piepmeier, S. Yueh, D. Entekhabi, M. H. Cosh, T. Caldwell, J. Walker, X. Wu, A. Berg, T. Rowlandson, A. Pacheco, H. McNairn, M. Thibeault, J. Martínez-Fernández, Á. González-Zamora, M. Seyfried, D. Bosch, P. Starks, D. Goodrich, J. Prueger, M. Palecki, E. E. Small, M. Zreda, J.-C. Calvet, W. T. Crow, and Y. Kerr</i> 4994 |
| Radar Systems | |
| Incoherent Target Scattering Decomposition of Polarimetric SAR Data Based on Vector Model Roll-Invariant Parameters | <i>H. Aghababae and M. R. Sahebi</i> 4392 |
| Spectral Processing for Step Scanning Phased-Array Radars | <i>L. Borowska, G. Zhang, and D. S. Zrnic</i> 4534 |
| A Parameterized ASCAT Measurement Spatial Response Function | <i>R. D. Lindsley, C. Anderson, J. Figa-Saldaña, and D. G. Long</i> 4570 |
| Dual-Polarization Radar Characteristics of Wind Turbines With Ground Clutter and Precipitation | <i>R. M. Beauchamp and V. Chandrasekar</i> 4833 |
| Synthetic Aperture Radar | |
| Calibration of Compact Polarimetric SAR Images Using Distributed Targets and One Corner Reflector | <i>H. Tan and J. Hong</i> 4433 |
| Soil Moisture Retrieval in Agricultural Fields Using Adaptive Model-Based Polarimetric Decomposition of SAR Data | <i>L. He, R. Panciera, M. A. Tanase, J. P. Walker, and Q. Qin</i> 4445 |

| | | |
|---|--|------|
| Sea Ice Concentration Estimation During Melt From Dual-Pol SAR Scenes Using Deep Convolutional Neural Networks: A Case Study | <i>L. Wang, K. A. Scott, L. Xu, and D. A. Clausi</i> | 4524 |
| Spaceborne Synthetic Aperture Radar Data Focusing on Multicore-Based Architectures | <i>P. Imperatore, A. Pepe, and R. Lanari</i> | 4712 |
| An Efficient Solution to the Factorized Geometrical Autofocus Problem | <i>J. Torgrimsson, P. Dammert, H. Hellsten, and L. M. H. Ulander</i> | 4732 |
| Target Classification Using the Deep Convolutional Networks for SAR Images. | <i>S. Chen, H. Wang, F. Xu, and Y.-Q. Jin</i> | 4806 |
| InSAR-Based Model Parameter Estimation of Probability Integral Method and Its Application for Predicting Mining-Induced Horizontal and Vertical Displacements | <i>Z. F. Yang, Z. W. Li, J. J. Zhu, J. Hu, Y. J. Wang, and G. L. Chen</i> | 4818 |
| A Multibaseline Pol-InSAR Inversion Scheme for Crop Parameter Estimation at Different Frequencies. | <i>M. Pichierri, I. Hajnsek, and K. P. Papathanassiou</i> | 4952 |
| Global Navigation Satellite System | | |
| Wind Speed Retrieval Algorithm for the Cyclone Global Navigation Satellite System (CYGNSS) Mission | <i>M. P. Clarizia and C. S. Ruf</i> | 4419 |
| Evapotranspiration Variations in the Mississippi River Basin Estimated From GPS Observations | <i>T. Zhang and S. Jin</i> | 4694 |
| Determination of Differential Code Bias of GNSS Receiver Onboard Low Earth Orbit Satellite | <i>J. Zhong, J. Lei, X. Yue, and X. Dou</i> | 4896 |
| Lidar Systems | | |
| Robust Segmentation for Large Volumes of Laser Scanning Three-Dimensional Point Cloud Data. | <i>A. Nurunnabi, D. Belton, and G. West</i> | 4790 |
| UV/Visible/Infrared Imagers | | |
| A Physics-Based Method to Retrieve Land Surface Temperature From MODIS Daytime Midinfrared Data | <i>B.-H. Tang and J. Wang</i> | 4672 |
| A Comparison of Tropical Rainforest Phenology Retrieved From Geostationary (SEVIRI) and Polar-Orbiting (MODIS) Sensors Across the Congo Basin | <i>D. Yan, X. Zhang, Y. Yu, and W. Guo</i> | 4867 |
| Satellite Systems | | |
| Estimation of ATMS Antenna Emission From Cold Space Observations. | <i>H. Yang, F. Weng, and K. Anderson</i> | 4479 |
| Relative Trajectory Estimation During Chang'e-2 Probe's Flyby of Asteroid Toutatis Using Dynamics, Optical, and Radio Constraints | <i>Y. Bu, W. Tang, W. Fa, C. Ding, G. Tang, Y. Yang, J. Cao, H. Chen, and H. Yin</i> | 4680 |
| Cross-Calibration of GF-1 PMS Sensor With Landsat 8 OLI and Terra MODIS. | <i>H. Gao, X. Gu, T. Yu, Y. Sun, and Q. Liu</i> | 4847 |

About the Cover: The cover describes the Advanced Technology Microwave Sounder (ATMS) onboard the Suomi NPP satellite, including (top) a schematic of the antenna subsystem (left) and a sketch plot for polarization direction definition by taking the scan plane and the reflection plane as reference frames, respectively (right). An example of the SNPP ATMS orbital brightness temperatures at channel 18 on February 20, 2012 is also depicted at the bottom. For more information please see ‘‘Estimation of ATMS Antenna Emission From Cold Space Observations,’’ by Yang *et al.*, which begins on page 4479.